Electrochimica Acta 146 (2014) 395–402

Contents lists available at ScienceDirect

Electrochimica Acta

journal homepage: www.elsevier.com/locate/electacta

Comparative Study of TiS_2/Li-In All-Solid-State Lithium Batteries Using Glass-Ceramic Li_3PS_4 and $Li_{10}GeP_2S_{12}$ Solid Electrolytes

Bum Ryong Shin, Young Jin Nam, Dae Yang Oh, Dong Hyeon Kim, Jin Wook Kim, Yoon Seok Jung*

School of Energy and Chemical Engineering, Department of Energy Engineering, Ulsan National Institute of Science and Technology (UNIST), Ulsan 689-798, Korea

ARTICLE INFO

Article history:
Received 11 June 2014
Received in revised form 25 August 2014
Accepted 26 August 2014
Available online 21 September 2014

Keywords:
Batteries
Solid electrolyte
All-solid-state batteries
Electrodes

ABSTRACT

A systematic investigation on the electrochemical performances of all-solid-state TiS_2/Li-In cells with various configurations using glass-ceramic Li_3PS_4 (LPS) and $Li_{10}GeP_2S_{12}$ (LGPS) solid electrolytes is presented. In spite of the superior conductivity of LGPS to that of LPS, LGPS shows poor stability in the low voltage range below ~1 V (vs. Li/Li$^+$) as evidenced by cyclic voltammetry (CV) and *ex-situ* XRD experiments. The combined use of the LGPS cathode layer and an LGPS-LPS SE bilayer where LPS forms an interface with the Li-In anode ((TiS$_2$-LGPS)/(LGPS-LPS)/Li-In cell) results in the best overall performance at 30 °C, exhibiting a capacity of ~60 mA h g^{-1} (~25% of the theoretical capacity) at 20C, over a voltage range of 1.5–3.0 V (vs. Li/Li$^+$). Combined analyses by electrochemical impedance spectroscopy (EIS) and conductivity measurements of the cathode layers highlight the importance of having an SE of high conductivity and optimizing the structure of the composite electrode.

1. Introduction

Conventional lithium-ion batteries (LIBs) utilize organic liquid electrolytes in which lithium salts are dissolved in organic alkyl carbonate solvents [1]. Not only flammability but also possible leakage of the organic liquid electrolyte in LIBs causes serious safety concern [1–3]. Recently, all-solid-state lithium batteries (ASSLBs) using inorganic solid electrolytes (SEs) have been seriously considered for large-scale energy-storage applications in devices such as electric vehicles and smart grids, because of their inherent safety [1,4,5]. Although thin-film ASSLBs using LiPON ($Li_{3.3}PO_{3.9}N_{0.17}$) have been reported to show excellent cycle performance [6,7], their large-scale application is not feasible because of the expensive vacuum-deposition process required for fabrication [6,7]. Alternatively, sulfide SE materials provide promising advantages for commercialization of large-scale ASSLBs. Several sulfide SEs have been developed that display high ionic conductivity on the order of 10^{-3}–10^{-2} S cm^{-1}, which is similar to that of conventional organic liquid electrolytes [4,5,8–10]. Moreover, sulfide SE materials exhibit ductility, displaying Young's moduli between those of typical oxide ceramics and organic polymers [3,11]. The high ionic conductivity and ductility of sulfide SEs enable the realization of bulk-type (or composite-type) all-solid-state batteries in which the electrode layer is formed by simply cold pressing a mixture of the active powders, SE powders, and conductive carbon [3–5,11].

The choice of SE makes a significant impact on the performance of ASSLBs, with ionic conductivity being of prime importance. The Kanno group reported thio-LISICON ($Li_{3.25}Ge_{0.25}P_{0.75}S_4$) [8] SE displaying conductivities up to 2.2×10^{-3} S cm^{-1} and LGPS ($Li_{10}GeP_2S_{12}$) [4] SE displaying conductivities up to 1.2×10^{-2} S cm^{-1}. Conductivities over 10^{-3} S cm^{-1} have also been demonstrated using xLi_2S-(100-x)P_2S_5 glass-ceramic (GC) SEs by the Tatsumisago group [9], who recently reported that the conductivity of $70Li_2S$-$30P_2S_5$ GC SE can be further enhanced to 1.7×10^{-2} S cm^{-1} by minimizing the grain boundary interface resistance via hot-pressing [5]. Since ionic conductivity of 1×10^{-2} S cm^{-1} is equal to that of organic liquid electrolytes used in conventional lithium-ion batteries (LIBs) and the transference number of Li$^+$ ions in the SE is unity, the performance of ASSLBs should be competitive to that of conventional LIBs. However, ionic conduction pathways in ASSLBs are more complicated than those in conventional LIBs. While liquid electrolytes can wet almost all surfaces of the active materials, the contacts between SEs and the active materials are highly dependent on factors such as the particle size distribution and mixing conditions [12]. In some cases, desired electronic conduction pathways are overtaken by poor ionic conduction pathways [12]. Therefore, the ionic conductivity of SEs is not directly proportional to the performance of ASSLBs. In this regard, a systematic investigation on the

* Corresponding author. Tel.: +82-52-217-2944; fax: +82-52-217-3009.
E-mail address: ysjung@unist.ac.kr (Y.S. Jung).

http://dx.doi.org/10.1016/j.electacta.2014.08.139
0013-4686/

effects of the configuration of all-solid-state cells on their performance is needed. Electrochemical stability of SEs is another critical factor that restricts the choice of possible electrode materials and affects the cycle performance and kinetic properties of all-solid-state cells [13–17], as observed in conventional LIBs [18,19]. For example, Li_xMO_2 (M = Co, Ni, Mn, etc., $0 \le x \le 1$) cathode materials used in conventional LIBs show poor performance originating from the low oxidation onset potential of sulfide SEs (~3 V vs. Li/Li^+) [15–17] and incompatibility with the sulfide SE [14]. Stable metal oxide coatings, such as $Li_4Ti_5O_{12}$ [14], $LiNbO_3$ [4,20], Li-Si-O [15], Al_2O_3 [21], and $BaTiO_3$ [22], are necessary to reduce large charge transfer resistances at the interface between the sulfide SE and oxide cathode. The underlying mechanism can be explained in terms of blocking of interatomic diffusion [23] or suppression of the formation of a space charge layer in the sulfide SE [14,22]. Use of sulfide-based cathode materials can avoid the instability problem of sulfide SEs because of low operating voltages (<~3 V vs. Li/Li^+). In previous reports, TiS_2 was demonstrated to exhibit capacity close to the theoretical one ($TiS_2 + Li^+ + e^- \rightarrow LiTiS_2$, 239 mA h g^{-1}) with excellent durability [12]. Recently, our group also reported that $LiTi_2(PS_4)_3$ formed a favorable interface with $75Li_2S$-$25P_2S_5$ GC SEs, leading to stable cycle performance [17].

In this study, the performances of all-solid-state TiS_2/Li-In cells with various configurations were systematically investigated using two different SEs: GC Li_3PS_4 (LPS) and LGPS. Cyclic voltammetry (CV) and *ex-situ* X-ray diffraction (XRD) results confirmed that the higher conductivity of LGPS compared to that of LPS is negated by poor stability in the negative voltage range. The use of an LGPS-LPS SE bilayer in which LPS forms an interface with the Li-In anode is demonstrated to optimize battery performances in terms of stability and rate capability. Additionally, the effects of composition and loading of the cathode layer are compared by measuring Li^+ ion- and electronic conductivities.

2. Experimental

Preparation of LPS and LGPS SE powders – LPS (or $75Li_2S$-$25P_2S_5$) GC SE powders were prepared by mechanical milling and subsequent heat-treatment [17]. 2 g of batches of Li_2S (99.9%, Alfa Aesar) and P_2S_5 (99%, Sigma Aldrich) mixture were mechanically milled at 500 rpm for 10 h at room temperature using a planetary ball mill (Pulverisette 7PL; Fritsch GmbH) with a ZrO_2 vial (80 mL) and 115 g of ZrO_2 balls (5 mm in diameter). The obtained glass powders were put into a glass ampoule and sealed under vacuum (≤40 Pa). The sealed ampoule was subjected to heat treatment at 243 °C for 1 h. For the preparation of LGPS powders, stoichiometric amounts of Li_2S, P_2S_5, and GeS_2 (99.9%, American Elements) powders were thoroughly mixed using a Thinky Mixer (AR-100, THINKY Inc.) with a plastic vial (12 mL) and eight ZrO_2 balls (5 mm in diameter) at 2000 rpm (33 s^{-1}) for 30 min. The mixed powders pelletized under 360 MPa were put into a quartz tube and sealed under vacuum (≤40 Pa). The sealed quartz tube was subjected to heat treatment at 550 °C for 10 h with ±1 °C min^{-1}.

Materials characterization – For the XRD analyses, a specially designed cell was used, in which the air-sensitive SE powders or disassembled pelletized cells were placed on a beryllium window and hermetically sealed inside the Ar-filled dry box. Then, the prepared XRD cell was mounted on a D8-Bruker Advance diffractometer equipped with Cu K_α radiation (1.54056 Å). All the XRD patterns were recorded at 40 kV and 40 mA using a continuous scanning mode at 1.5° min^{-1}. Field emission scanning electron microscopy (FESEM) images were obtained using S-4800 (Hitachi).

Electrochemical characterization – Measurements of Li^+ ion conductivity and electronic conductivity of the SEs were carried out by AC method and DC method using a Li^+ ion blocking cell (Ti/SE/Ti) at 30 °C, respectively. For the CV experiments, Ti/SE/$Li_{0.5}$In cells were constructed. Li^+ ion conductivity and CV data obtained by using 30 μm thick Au film (Au/SE/Au for AC method and Au/SE/$Li_{0.5}$In for the CV experiments) matched perfectly with the data using Ti electrodes, confirming that Ti acts as an inert electrode. After 150 mg of SE powders were pelletized under 370 MPa for 5 min, 100 mg of a partially lithiated indium ($Li_{0.5}$In, nominal composition) powders prepared by mechanically milling the mixture of In (Aldrich, 99.99%, containing Mg) and Li (FMC Lithium corp.) powders were put on one side of the as-formed SE pellet and pressed under 370 MPa for 3 min. The scan rate was 0.2 mV s^{-1}. For fabrication TiS_2/$Li_{0.5}$In all-solid-state cells, composite electrodes were prepared by manually mixing the TiS_2 (99.9%, Aldrich, 200 mesh) and SE powders. Note that no conductive additive is required because TiS_2 is metallic [12,24]. The weight ratio of the TiS_2/SE was 0.5. SE pellets were formed by pressing 150 mg of the SE powders at 74 MPa. TiS_2 composite electrode materials (10 mg) were then carefully spread on the top of the SE layer and the cell was pelletized by pressing at 370 MPa for 3 min. Finally, 50 mg of the prepared $Li_{0.5}$In powders were attached to the back SE face at 370 MPa for 3 min. All pressings were carried out in a polyaryletheretherketone (PEEK) mold (diameter = 13 mm) with Ti metal rods as current collectors for both the working and counter/reference electrodes. All the processes for preparing the SEs and fabricating the all-solid-state cells were performed in an Ar-filled dry box. The galvanostatic discharge–charge cycling of the all-solid-state cells was performed between 1.5 and 3.0 V (*vs.* Li/Li^+) at 30 °C. The capacity is based on the weight of TiS_2. The electrochemical impedance spectroscopy (EIS) study was performed using an Iviumstat (IVIUM Technologies Corp.). The AC impedance measurements were recorded using a signal with an amplitude of 10 mV and a frequency range from 500 kHz to 5 mHz. The cells were discharged to 2.1 V (*vs.* Li/Li^+) at 50 mA g^{-1} and a constant voltage of 2.1 V was applied with a limiting current of 12.5 mA g^{-1}. Then, the cell was allowed to rest for approximately 3 h before the EIS measurements. In order to measure Li^+ ion conductivity of the TiS_2/SE electrode, specially designed electron-blocking symmetric cell of Li/SE/electrode/SE/Li by DC and AC methods [25].

3. Results and discussion

Fig. 1a and b shows FESEM images of the as-prepared LPS (Li_3PS_4 or $75Li_2S$-$25P_2S_5$ GC) and LGPS SE powders. Both of the SE powders are a few to tens of μm size with irregular morphology. Fig. 1c shows XRD patterns of the LPS and LGPS SE pellets. The peaks of LPS match well with previous reports [26]. The as-prepared LGPS exhibits characteristic peaks (denoted '◊') corresponding to the tetragonal $Li_{10}GeP_2S_{12}$ with a space group of $P4_2/nmc$ [27] along with minor impurity peaks (denoted '?'). XRD data of LGPS that was obtained from rotating XRD cells (15 rpm) exactly matches with the one without rotation, confirming that any preferred crystal orientation does not occur during the cold pressing process for fabricating the SE pellets. Fig. 1d displays the Nyquist plots of Ti/SE/Ti cells measured by the AC method. The intercept at the x-axis equals the SE resistance, which can be converted to electrical conductivity. As electronic conductivities of LPS and LGPS measured by the DC method are on the order of 1×10^{-8} S cm^{-1}, electrical conductivities obtained by the AC method are directly assigned as Li^+ ionic conductivities. At 30 °C, the LPS and LGPS exhibit conductivities of 1.0×10^{-3} S cm^{-1} and 6.3×10^{-3} S cm^{-1}, respectively. The LGPS conductivity (6.3×10^{-3} S cm^{-1}) is approximately half of the previously reported value (1.2×10^{-2} S cm^{-1}) [4], which is a result of using a cold pressed pellet in this work as grain boundary resistances that originate from voids in the pellet work to lower the overall conductivity [5]. The presence of minor impurities, seen in the XRD pattern, may also contribute the decrease in conductivity.

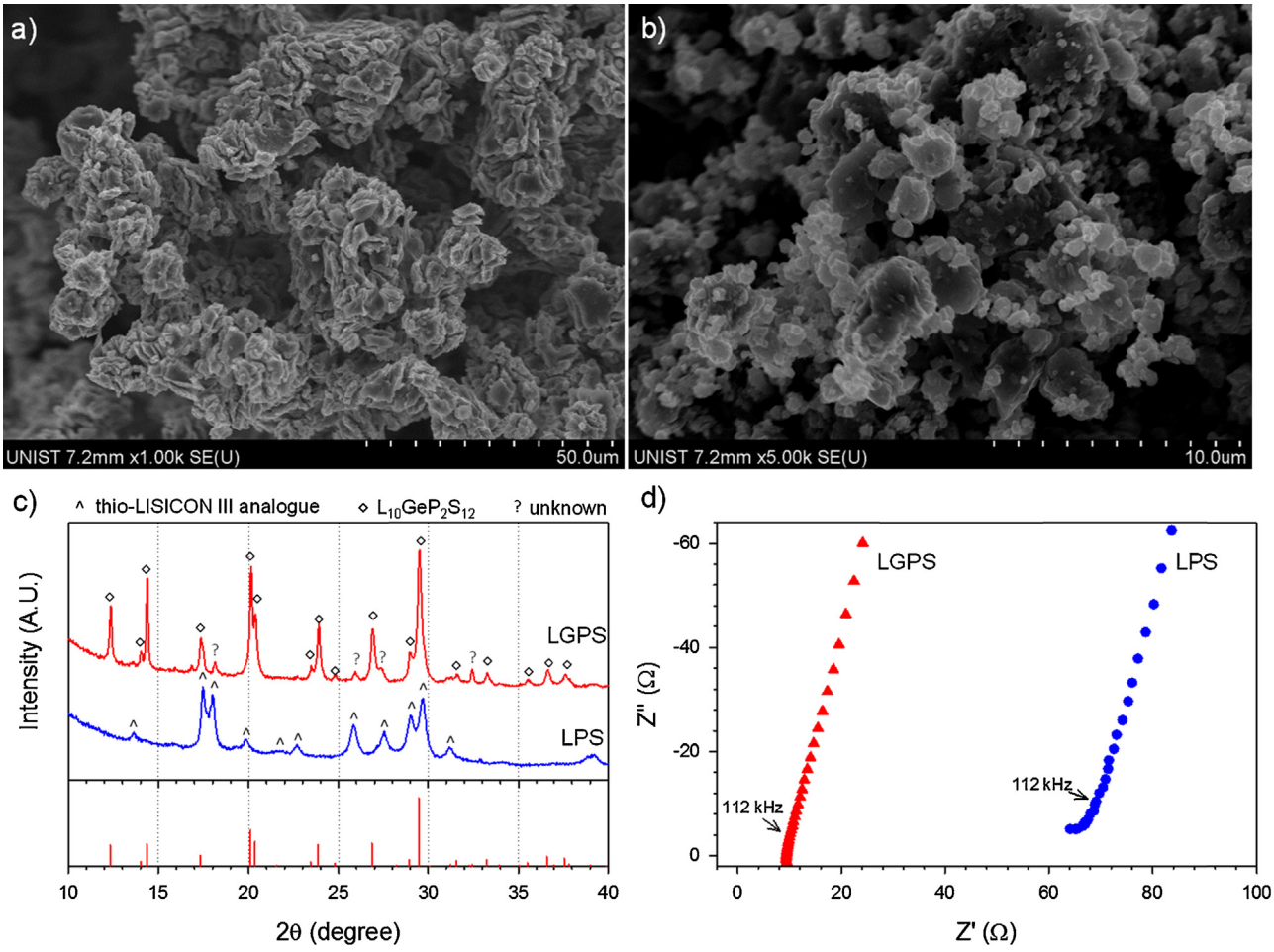

Fig. 1. FESEM images of a) glass-ceramic Li_3PS_4 (LPS) and b) $Li_{10}GeP_2S_{12}$ (LGPS) solid electrolyte (SE) powders. c) XRD patterns of LPS and LGPS SE pellets. XRD reference peaks of LGPS are also shown at the bottom [27]. d) Nyquist plot of Ti/SE/Ti cells at 30 °C.

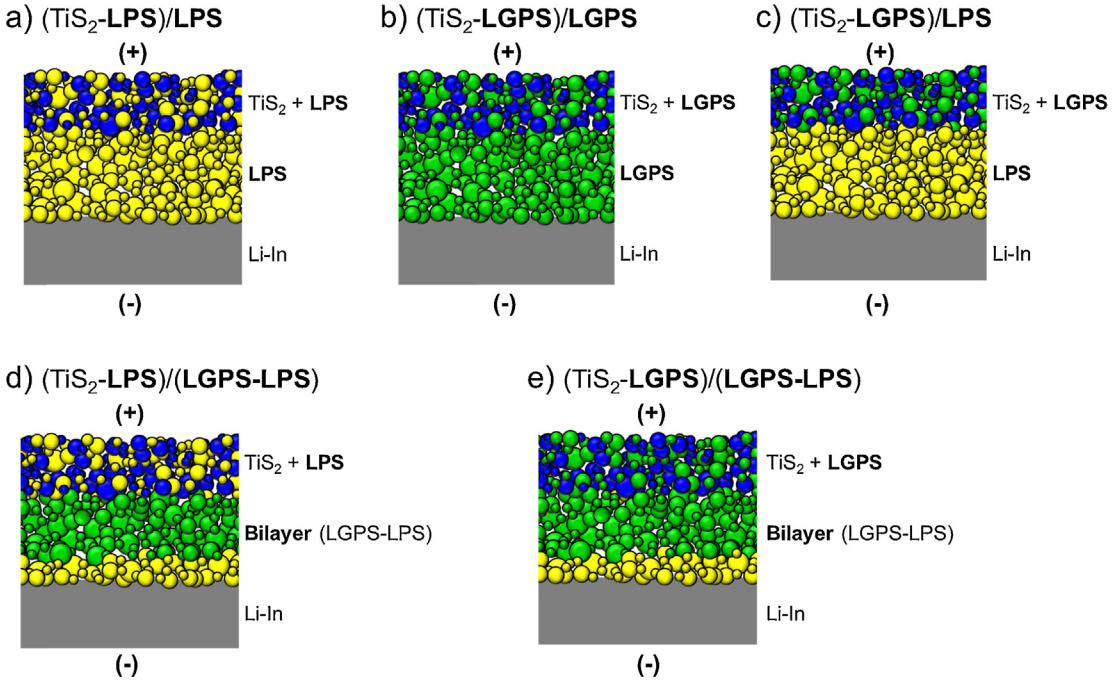

Fig. 2. Schematic diagram of the TiS_2/Li-In all solid-state cells with five different combinations of the SEs used in the TiS_2 composite cathodes and the SE layers.

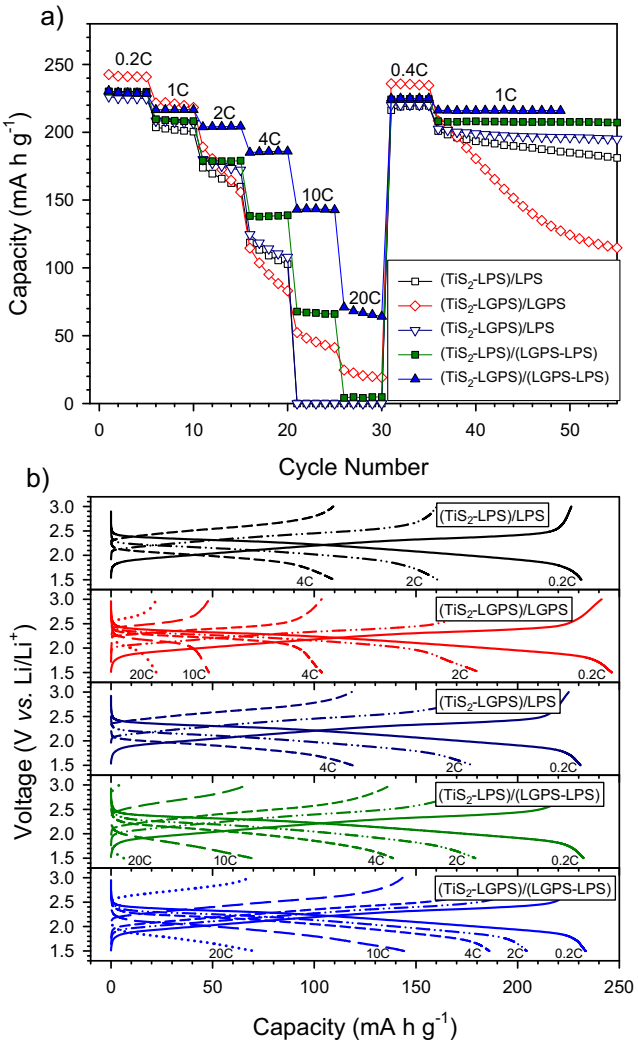

Fig. 3. a) Variations in charge capacities versus cycle number and b) charge-discharge voltage profiles for the TiS_2/Li-In all-solid-state cells cycled at different rates between 1.5 and 3.0 V (vs. Li/Li^+) at 30 °C. Five different configurations of cathode layer/SE layer are represented. For example, in the (TiS_2-LGPS)/LPS cell, LGPS and LPS were used in the cathode layer and SE layer, respectively. An SE layer comprising a double layered LGPS-LPS where LGPS forms an interface with the cathode layer is denoted as bilayer.

For this study, TiS_2 was chosen as the cathode material because of its metallic properties and highly reversible reaction with Li [12,24,25]. Importantly, a mild operating voltage of ~2.1 V (vs. Li/Li^+) lies within the electrochemical window of sulfide SEs [17,20]. The cathode was composed of a 10 mg mixture of TiS_2 and SE with a weight ratio of 0.5 (TiS_2/SE). The all-solid-state TiS_2/Li-In cells were cycled at different rates between 1.5 and 3.0 V (vs. Li/Li^+) at 30 °C. Fig. 2 represents schematic diagrams of the TiS_2/Li-In cells with different combinations of SEs in the composite cathode layer and the SE layer. Fig. 3 shows the varying performance with each permutation. In Fig. 3a, at 0.2C (= 126 μA cm^{-2} = 50 mA (g of TiS_2)$^{-1}$), the capacities are close to the theoretical value of TiS_2 (239 mA h g^{-1}) [24]. As shown in Fig. 3b, polarization increases, and capacity correspondingly decreases at higher C-rates. In Fig. 3a, the (TiS_2-LPS)/LPS cell, in which LPS is used in both the cathode layer and the SE layer, displays a negligible capacity starting at 10C. In contrast, the (TiS_2-LGPS)/LGPS cell exhibits better rate capability and does not reach zero capacity. This result is not surprising as the conductivity of LGPS is six times higher than that of LPS. However, after 35 cycles at 1C, the capacity of the (TiS_2-LGPS)/LGPS cell decays rapidly. This degradation is believed to be associated with the instability of LGPS when in contact with the Li-In anode, details of which are discussed elaborately later. When an LPS SE layer is used in place of the LGPS SE layer in the (TiS_2-LGPS)/LGPS cell, designated (TiS_2-LGPS)/LPS, the capacity degradation problem is avoided. Compared to the (TiS_2-LPS)/LPS cell, the (TiS_2-LGPS)/LPS cell shows slightly improved performance, which indicates that the conductance of the SE layer rather than that of the cathode layer is rate determining when an LPS SE layer is employed.

To prevent direct contact between LGPS and the Li-In anode while maximizing the conductance of the SE layer, an LGPS-LPS SE bilayer where LPS forms an interface with the Li-In anode was constructed with a 4.0 LGPS/LPS weight ratio [16,28]. While no capacity is exhibited at 10C for the (TiS_2-LPS)/LPS cell, the (TiS_2-LPS)/(LGPS-LPS) cell exhibits ~60 mA h g^{-1} at 10C, which is attributed to the tripled conductance from 1.9×10^{-2} S for the LPS SE layer to 8.0×10^{-2} S for the LGPS-LPS bilayer. Replacement of LPS in the (TiS_2-LPS)/(LGPS-LPS) cell with LGPS, designated (TiS_2-LGPS)/(LGPS-LPS), further improves the rate capability, delivering ~60 mA h g^{-1} even at 20C. From this observation, it is concluded that, when Li^+ ion conductance in the SE layer is high enough, the ionic conduction of the cathode layer governs the overall kinetics of the solid-state cell, as seen with the bilayer configuration. Considering that thickness of the SE layer must be significantly reduced from ~700 μm (150 mg for disc with 13 mm of diameter) to a more realistic value (e.g. less than ~100 μm) and the amount of cathode material must be increased to obtain a high energy density based on the total mass or volume of the pelletized cell, the results depicted in Fig. 3 imply that the rate determining step is Li^+ ion transport in the cathode layer rather than in the SE layer. Therefore, it is of critical importance to enhance the conductivity of SE materials further and optimize electrode structures for maximizing ionic conduction pathways.

To analyze the kinetic properties of the cells in detail, the EIS measurements were conducted at the 1st and 30th cycles. The EIS spectra shown in Fig. 4a comprises three parts. The first resistance value, R_1, represents the resistance of the SE layer [15,17]. It is seen that the R_1 values for the (TiS_2-LPS)/LPS and (TiS_2-LGPS)/LPS cells in Fig. 3a match the resistance of LPS obtained by the Ti/SE/Ti cell in Fig. 1b. The second resistance value, R_2, originates from the charge transfer resistances from TiS_2/SE and SE/Li-In interfaces [15,17]. The sloping tails at low frequency are attributed to Li^+ diffusion in TiS_2 [29]. The R_1 and R_2 values from the EIS spectra in Fig. 4a are summarized in Fig. 4b and contain several notable features. First, when LPS is used for the SE layer, the contribution of R_2 to the overall resistance is minor. This behavior is in accordance with the observation in Fig. 3a in that the (TiS_2-LGPS)/LPS cell shows a similar rate capability to that of the (TiS_2-LPS)/LPS cell. In sharp contrast, when the highly conductive LGPS or LGPS-LPS bilayer is used as the SE layer, the contribution of R_2 to the overall resistance becomes critical, which matches with the behavior of the (TiS_2-LPS)/(LGPS-LPS) cell vs. the (TiS_2-LGPS)/(LGPS-LPS) cell in Fig. 3a. Second, after 30 cycles, increases in both R_1 and R_2 values are observed. These increases may be associated with loosened contacts between particles brought about by dimensional changes of TiS_2 upon Li^+ insertion/extraction (12% of volume change = $\frac{\text{Molar volume of } LiTiS_2 - \text{Molar volume of } TiS_2}{\text{Molar volume of } TiS_2} \times 100$, based on the crystallographic data of TiS_2 (JCPDS No. 15-0853) and $LiTiS_2$ (JCPDS No. 28-0595)) and/or instability at the TiS_2/SE and SE/Li-In interfaces [17]. Although clear explanation is not possible, the increases of R_1 values after cycles may be associated with the increase of grain boundary resistance of the SE layer. Possible mechanical degradation of the cold-pressed SE pellet caused by effects of the dimensional changes of active materials is postulated to contribute to the increase of grain boundary resistance. Importantly,

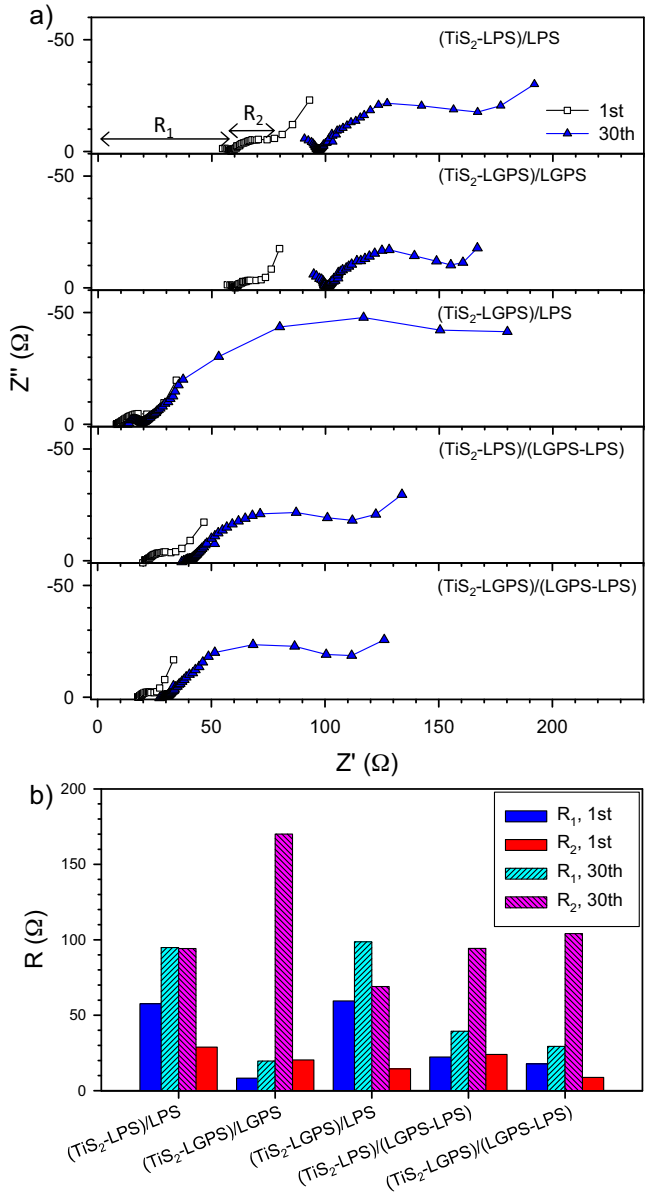

Fig. 4. a) Nyquist plots of TiS_2/Li-In all-solid-state cells with five different configurations of cathode layer/SE layer at the 1st and 30th cycle at 30 °C. b) R values obtained from the Nyquist plots in a. The R terms are explained in the main text.

it should be noted that the increase in R_2 is the highest for the (TiS_2-LGPS)/LGPS cell, which indicates the presence of an unstable interface between LGPS and Li-In.

The electrochemical stability of LPS and LGPS were evaluated using Ti/SE/Li-In cells by CV, as shown in Fig. 5. In the negative voltage range between 0.05 and 2.00 V (vs. Li/Li^+), a region where the deposition/dissolution of Li metal does not interfere with measurements, LGPS displays an appreciable amount of current (a few μA cm^{-2}) starting at ~1.0 V (vs. Li/Li^+), shown in Fig. 5a. Scanning further in the negative direction results in currents over 10 μA cm^{-2}, beginning at ~0.4 V (vs. Li/Li^+), and reaches 205 μA cm^{-2} at 0.05 V (vs. Li/Li^+). The irreversible reaction is not complete after the first cycle. From this result, it is evident that the LGPS has poor stability in the low potential range. In the positive voltage range, shown in Fig. 5b, both LPS and LGPS show onset potentials for irreversible oxidation starting at ~3.0 V (vs. Li/Li^+). However, the current densities are on the order of a few hundreds of nA cm^{-2}, which is much lower than the reduction current for the LGPS in the negative voltage range. Fig. 6 compares the performances of the (TiS_2-LGPS)/

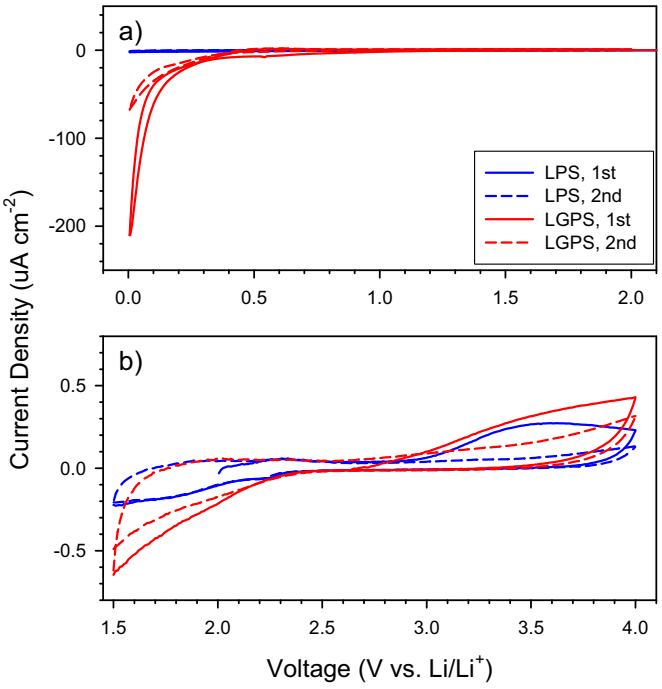

Fig. 5. First two cyclic voltammetry (CV) cycles of Ti/LPS/Li-In and Ti/LGPS/Li-In cells a) in the negative potential range and b) in the positive potential range at 30 °C. The scan rate was 20 mV s^{-1}.

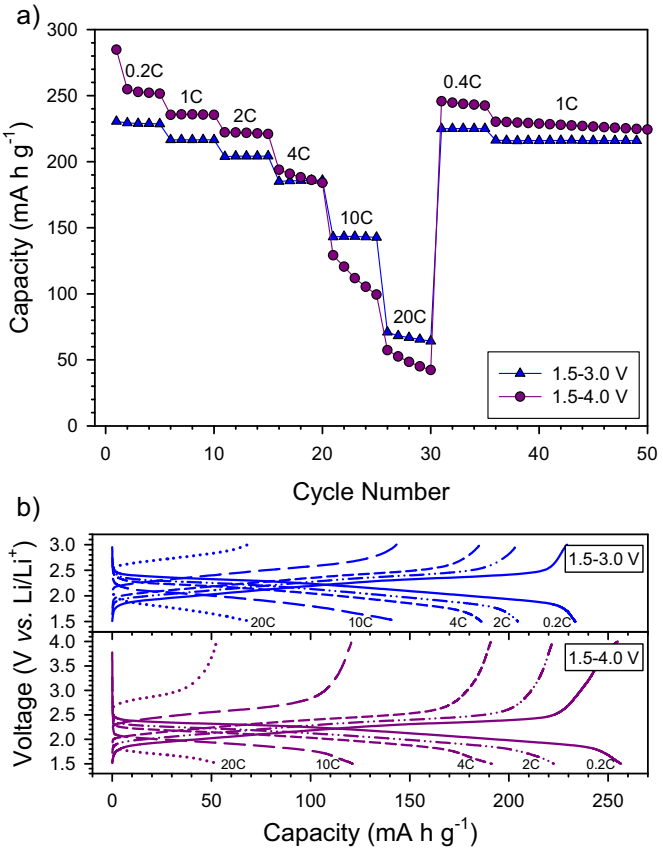

Fig. 6. a) Variations in charge capacity versus cycle number and b) charge-discharge voltage profiles for the TiS_2/Li-In all-solid-state cells with the (TiS_2-LGPS)/(LGPS-LPS) configuration cycled between 1.5–3.0 V and 1.5–4.0 V (vs. Li/Li^+) at 30 °C.

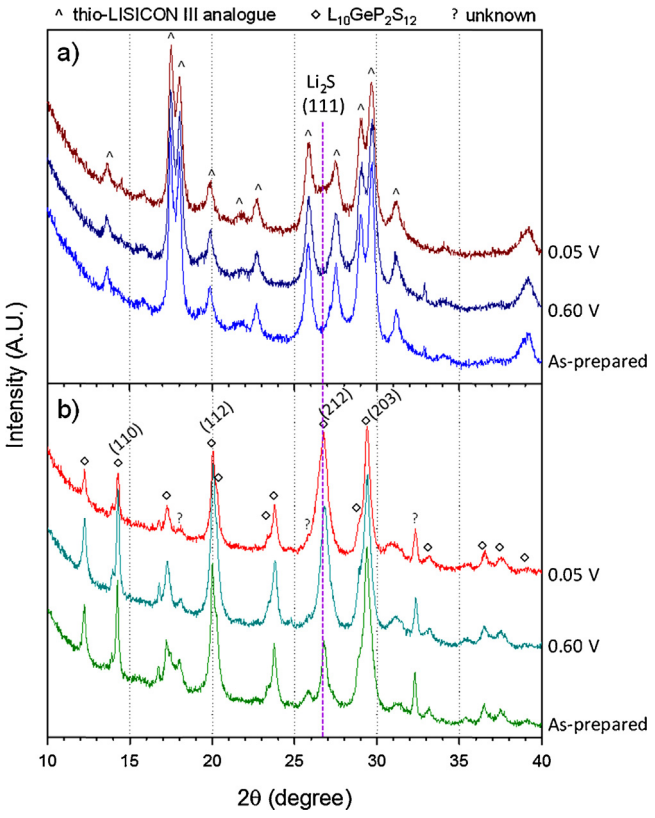

Fig. 7. *Ex-situ* XRD patterns of a) the LPS-carbon electrode and b) the LGPS-carbon electrode at the voltages (vs. L/Li$^+$) indicated.

(LGPS-LPS) between voltages windows of 1.5–4.0 V (vs. Li/Li$^+$) and 1.5– 3.0 V (vs. Li/Li$^+$). The increase in the upper cutoff voltage at 4.0 V leads to a just slight degradation in the rate performance. From this observation, the extremely poor performances occurred when the bare Li_xMO_2 cathode contacts with the sulfide SEs in many previous reports [15–17] are more related to the material incompatibility rather than the high operating potential itself. The material incompatibility can be explained by either the interatomic diffusion [23] or space charge layer increases the interfacial resistances [14,22].

The stability of the SE layer in the low voltage range was investigated by an *ex-situ* XRD experiment. To ensure that the amount of new phases formed by the electrochemical reaction was large enough to measure, a 10 mg mixture of carbon (super P) and SE powders at a 1:10 weight ratio was used as the working electrode. After reaching the designated voltage (0.05 or 0.6 V) through a negative voltage scan at 20 mV s^{-1}, the desired voltage was held constant for 3 h. Fig. 7 shows the *ex-situ* XRD patterns of LPS and LGPS after application of the voltage. The LPS-carbon electrode shows negligible change after discharge to 0.60 V (vs. Li/Li$^+$), which is equivalent to the operating voltage of the Li-In anode (In + Li$^+$ + e$^-$ ↔ LiIn) in the TiS_2/Li-In cells [30]. In sharp contrast, the intensity ratio for the characteristic peaks for the LGPS-carbon electrode changes significantly after discharge to 0.60 V (vs. Li/Li$^+$). Table 1 summarizes the intensity ratio of the (110), (112), (212), and (203) peaks. Further discharge to 0.05 V (vs. Li/Li$^+$) leads to larger changes in the intensity ratio, which indicates that a significant amount of the LGPS phase is altered. In particular, the gradual increase of the (212) peak upon discharge is notable. In contrast, the relative intensities for other (110) and (112) peaks are increased at 0.60 V and decreased at 0.05 V. It should be also pointed out that the (212) peak, centered at ~26.6°, is overlapped by the Li_2S (111) peak (JCPDS No. 23-0369). An increase in intensity at 26.6° is also found in the LPS-carbon electrode after an

Table 1
Relative intensity ratios of peaks obtained from *ex-situ* XRD experiments with the LGPS-carbon electrode, corresponding to Fig. 7.

	Relative intensity ratio[a]			
	(110)	(112)	(212)	(203)
As prepared	59	83	38	100
Discharged to 0.60 V	71	105	78	100
Discharged to 0.05 V	36	74	92	100

[a] The ratio was normalized by the intensity of the (203) peak.

applied voltage of 0.05 V, but not after 0.60 V. The formation of Li_2S can be explained by a reduction of the SE through the lithiation reaction [31]. The perovskite-type lithium lanthanum titanate, $Li_{3x}La_{2/3-2x}\square_{1/3-2x}TiO_3$ ($0 < x < 0.16$), is a well-studied oxide SE with a Li$^+$ ionic conductivity of 1×10^{-3} S cm^{-1} at room temperature [32]. However, at low potential or when in contact with Li metal Ti^{4+} is reduced to Ti^{3+}, resulting in a change to the electronic

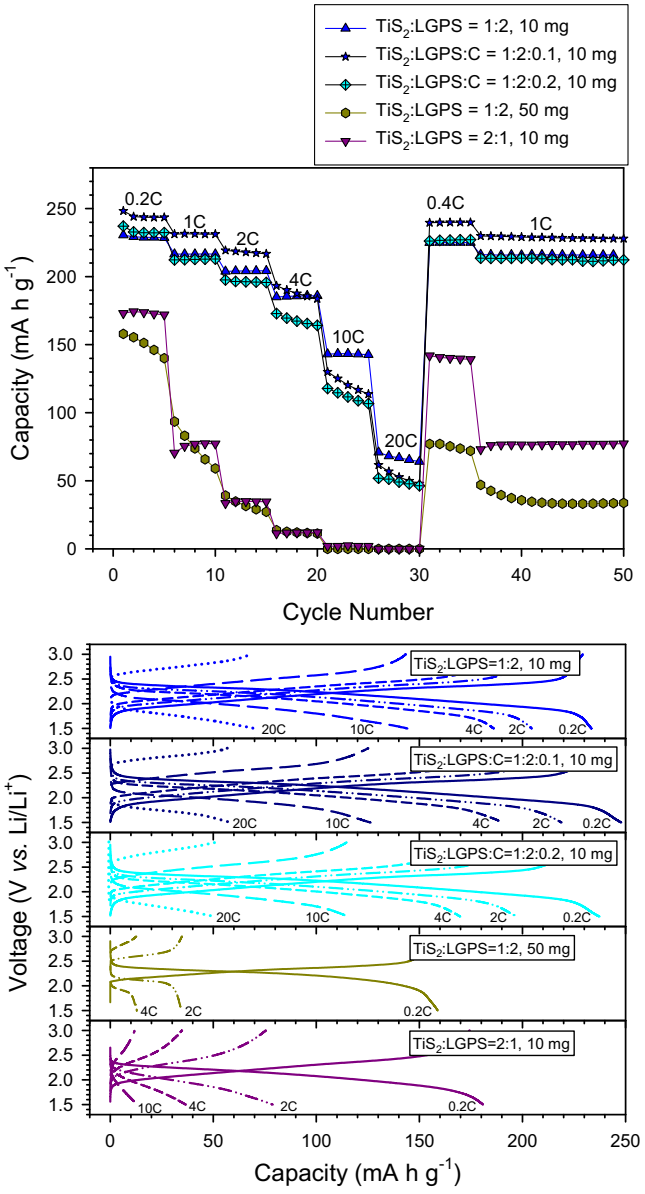

Fig. 8. a) Variations in charge capacity versus cycle number and b) charge-discharge voltage profiles for the TiS_2/Li-In all-solid-state cells with the (TiS_2-LGPS)/(LGPS-LPS) configuration cycled at different rates over two different voltage ranges at 30 °C. The weight ratio and the total weight of the cathode layer are shown.

Table 2
Li^+ ion conductivity/conductance and electronic conductivity of SE and the TiS_2/LGPS cathode layer used for ASSLB.

Sample	Weight ratio[a]	Weight of active material (mg)	Li^+ ion conductivity (S cm^{-1})	Li^+ ion conductance (S)	Electronic conductivity (S cm^{-1})
LPS	-	-	1.0×10^{-3}	1.9×10^{-2} (700)[b]	-
LGPS	-	-	6.3×10^{-3}	1.2×10^{-1} (670)[b]	-
LGPS-LPS bilayer	-	-	3.9×10^{-3}	8.0×10^{-2} (650)[b]	-
TiS_2	-	-	-	-	2.2×10^{2}
TiS_2-LGPS	0.5	3.3	4.8×10^{-4}	1.0×10^{-1} (64)[b]	5.6×10^{0}
		16.7		2.0×10^{-2} (320)[b]	
	2.0	6.7	1.5×10^{-5}	6.0×10^{-3} (33)[b]	1.1×10^{2}

[a] Weight ratio of TiS_2/LGPS.
[b] The value in parenthesis is the thickness of the electrode layer in μm.

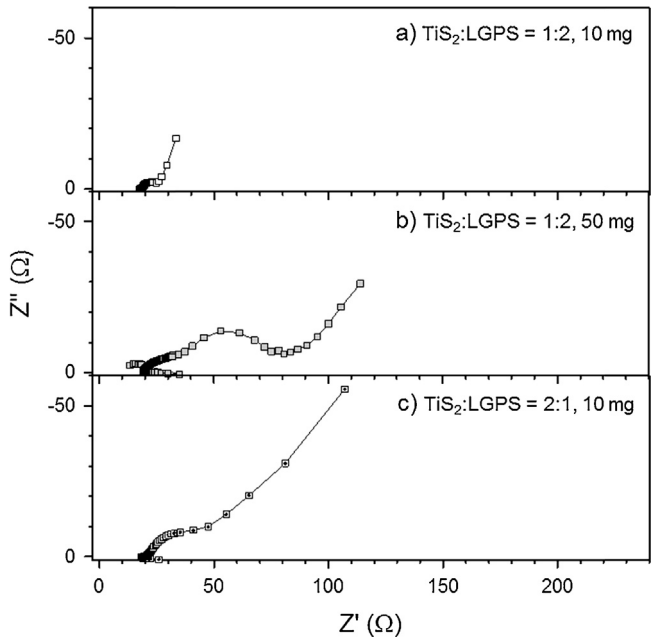

Fig. 9. Nyquist plots of TiS_2/Li-In all-solid-state cells with the (TiS_2-LGPS)/(LGPS-LPS) configuration of the first cycle at 30 °C. The weight ratio and the total weight of the cathode layer are shown.

conductivity [32]. To replace Ti, a fixed-valent, garnet-type $Li_7La_3Zr_2O_{12}$ was developed that is stable against reduction by Li metal [33]. Elemental Ge has also been investigated as an alternative anode material for LIBs because it reacts with a large amount of Li^+ ions in the range of ~0.2–0.5 V (vs. Li/Li^+) through an alloying/de-alloying reaction ($Ge + 4.4Li^+ + 4.4e^- \leftrightarrow Li_{4.4}Ge$, theoretical capacity = 1624 mA h g^{-1}) [34]. In this regard, it can be postulated that including Ge in the LGPS layer can promote reduction at low potentials. The instability of LGPS compared to LPS, demonstrated by CV and *ex-situ* XRD experiments, clearly corroborates the fast degradation of the (TiS_2-LGPS)/LGPS cell evidenced in Figs. 3 and 4.

To increase the energy density, either the weight fraction of TiS_2 or the total mass of the cathode layer should be increased. Fig. 8 compares effects on the rate performance of the cells with the (TiS_2-LGPS)/(LGPS-LPS) configuration at different weight fractions and total mass of the cathode layer. Effects of carbon additives were also investigated. Table 2 summarizes the Li^+ ionic conductivities/conductance and electronic conductivities of the SE, TiS_2, and TiS_2-LGPS cathode layers. As a result of the metallic nature of TiS_2, the TiS_2-LGPS electrode with a 0.5 TiS_2/LGPS weight ratio exhibits a high electronic conductivity of 5.6 S cm^{-1}. The addition of carbon additives slightly degrades the rate performance, which implies that the rate determining step in the electrode is the Li^+ ionic conduction, not the electronic conduction. The decreased rate is likely a result of carbon additives blocking the ionic conduction pathways [12]. As seen in Fig. 8, the increase in both the mass of the cathode layer to 50 mg and the weight fraction of TiS_2 to 2.0 (TiS_2/LGPS) significantly lowers the capacity. In both cases, significant increases in interfacial charge transfer resistance are observed in the Nyquist plots, shown in Fig. 9. In Table 2, the conductance values for the 50 mg electrode with a 0.5 TiS_2/LGPS weight ratio (1.0×10^{-2} S) and for the 10 mg electrode with a 2.0 TiS_2/LGPS weight ratio (6.0×10^{-3} S) are approximately one order of magnitude lower than the value of the 10 mg electrode with a 0.5 TiS_2/LGPS weight ratio (1.0×10^{-1} S), which corroborates the rate performances shown in Fig. 8. Considering cell performances vary depending on the loading and the composition of the electrode, strategic design of a composite electrode for an all-solid-state cell is critical for the formation of favorable conduction pathways. Measurements of electrode conductance can be used to predict and/or analyze the kinetic properties and thus this method is useful for the design of composite electrodes for all-solid-state cells.

4. Conclusion

The electrochemical performances of all-solid-state TiS_2/Li-In cells with various configurations using two different SEs (LPS and LGPS) were systematically investigated. Although LGPS exhibited a higher conductivity (6.2×10^{-3} S cm^{-1}) than LPS (1.0×10^{-3} S cm^{-1}), LGPS suffered from poor stability in the low voltage range as evidenced by CV and *ex-situ* XRD experiments, which resulted in a severe capacity fading of the TiS_2/Li-In cell. Optimization of the cell configuration was achieved by using LGPS in the cathode layer and an LGPS-LPS SE bilayer where LPS forms an interface with the Li-In anode ((TiS_2-LGPS)/(LGPS-LPS)/Li-In cell), showing a capacity of ~60 mA h g^{-1} (~25% of the theoretical capacity) at 20C between 1.5 and 3.0 V (vs. Li/Li^+) at 30 °C. When a highly conductive LGPS-LPS SE bilayer is used, it appears that the rate determining step is ionic conduction in the cathode layer. This work highlights the importance of further development of highly conductive SE layers and design of composite electrode structures.

Acknowledgement

This work was supported by the Energy Efficiency & Resources Program of the Korea Institute of Energy Technology Evaluation and Planning (KETEP) grant funded by the Korea government Ministry of Trade, Industry & Energy (No. 20112010100150), by the MSIP (Ministry of Science, ICT & Future Planning), Korea, under the C-ITRC (Convergence Information Technology Research Center) support program (NIPA-2014-H0301-14-1013) supervised by the NIPA (National IT Industry Promotion Agency), and by the Future Strategic Fund (1.130019.01) of UNIST (Ulsan National Institute of Science and Technology).

References

[1] J.B. Goodenough, Y. Kim, Chem. Mater. 22 (2010) 587.
[2] J.-M. Tarascon, M. Armand, Nature 414 (2001) 359.
[3] A. Hayashi, K. Noi, A. Sakuda, M. Tatsumisago, Nat. Commun. 3 (2012) 856.
[4] N. Kamaya, K. Homma, Y. Yamakawa, M. Hirayama, R. Kanno, M. Yonemura, T. Kamiyama, Y. Kato, S. Hama, K. Kawamoto, A. Mitsui, Nat. Mater. 10 (2011) 682.
[5] Y. Seino, T. Ota, K. Takada, A. Hayashi, M. Tatsumisago, Energy Environ. Sci. 7 (2014) 627.
[6] B. Wang, J.B. Bates, F.X. Hart, B.C. Sales, R.A. Zuhr, J.D. Robertson, J. Electrochem. Soc. 143 (1996) 3203.
[7] J.B. Bates, N.J. Dudney, B. Neudecker, A. Ueda, C.D. Evans, Solid State Ionics 135 (2000) 33.
[8] R. Kanno, M. Murayama, J. Electrochem. Soc. 148 (2001) A742.
[9] F. Mizuno, A. Hayashi, K. Tadanaga, M. Tatsumisago, Adv. Mater. 17 (2005) 918.
[10] G. Sahu, Z. Lin, J. Li, Z. Liu, N. Dudney, C. Liang, Energy Environ. Sci. 7 (2014) 1053.
[11] A. Sakuda, A. Hayashi, M. Tatsumisago, Sci. Reports 3 (2013) 2261.
[12] J.E. Trevey, C.R. Stoldt, S.-H. Lee, J. Electrochem. Soc. 158 (2011) A1282.
[13] R. Kanno, M. Murayama, T. Inaba, T. Kobayashi, K. Sakamoto, N. Sonoyama, A. Yamada, S. Kondo, Electrochem. Solid-State Lett. 7 (2004) A455.
[14] N. Ohta, K. Takada, L. Zhang, R. Ma, M. Osada, T. Sasaki, Adv. Mater. 18 (2006) 2226.
[15] A. Sakuda, H. Kitaura, A. Hayashi, K. Tadanaga, M. Tatsumisago, J. Electrochem. Soc. 156 (2009) A27.
[16] J.E. Trevey, Y.S. Jung, S.-H. Lee, Electrochim. Acta 56 (2011) 4243.
[17] B.R. Shin, Y.S. Jung, J. Electrochem. Soc. 161 (2014) A154.
[18] Y.S. Jung, A.S. Cavanagh, L.A. Riley, S.H. Kang, A.C. Dillon, M.D. Groner, S.M. George, S.H. Lee, Adv. Mater. 22 (2010) 2172.
[19] Y.S. Jung, P. Lu, A.S. Cavanagh, C. Ban, G.-H. Kim, S.-H. Lee, S.M. George, S.J. Harris, A.C. Dillon, Adv. Energy Mater. 3 (2013) 213.
[20] N. Ohta, K. Takada, I. Sakaguchi, L. Zhang, R. Ma, K. Fukuda, M. Osada, T. Sasaki, Electrochem. Commun. 9 (2007) 1486.
[21] J.H. Woo, J.E. Trevey, A.S. Cavanagh, Y.S. Choi, S.C. Kim, S.M. George, K.H. Oh, S.-H. Lee, J. Electrochem. Soc. 159 (2012) A1120.
[22] C. Yada, A. Ohmori, K. Ide, H. Yamasaki, T. Kato, T. Saito, F. Sagane, Y. Iriyama, Adv. Energy Mater. (2014), http://dx.doi.org/10.1002/aenm.201301416.
[23] A. Sakuda, A. Hayashi, M. Tatsumisago, Chem. Mater. 22 (2010) 949.
[24] M.S. Whittingham, Science 192 (1976) 1126.
[25] B.R. Shin, Y.J. Nam, J.W. Kim, Y.-G. Lee, Y.S. Jung, Sci. Reports 4 (2014) 5572.
[26] F. Mizuno, A. Hayashi, K. Tadanaga, M. Tatsumisago, Solid State Ionics 177 (2006) 2721.
[27] A. Kuhn, J. Koehler, B.V. Lotsch, Phys. Chem. Chem. Phys. 15 (2013) 11620.
[28] K. Takada, T. Inaba, A. Kajiyama, H. Sasaki, S. Kondo, M. Watanabe, M. Murayama, R. Kanno, solid State Ionics 158 (2003) 269.
[29] A.J. Bard, L.R. Faulkner, Electrochemical Methods: Fundamentals and Applications, 2nd ed., John Wiley & Sons, Inc, New York, 2001.
[30] Y.S. Jung, K.T. Lee, J.H. Kim, J.Y. Kwon, S.M. Oh, Adv. Funct. Mater. 18 (2008) 3010.
[31] S.P. Ong, Y. Mo, W.D. Richards, L. Miara, H.S. Lee, G. Ceder, Energy Environ. Sci. 6 (2013) 148.
[32] S. Stramare, V. Thangadurai, W. Weppner, Chem. Mater. 15 (2003) 3974.
[33] R. Murugan, V. Thangadurai, W. Weppner, Angew. Chem. Int. Ed. 46 (2007) 7778.
[34] J. Graetz, C.C. Ahn, R. Yazami, B. Fultz, J. Electrochem. Soc. 151 (2004) A698.